Materials Science and Engineering C 65 (2016) 109–115

Contents lists available at ScienceDirect

Materials Science and Engineering C

journal homepage: www.elsevier.com/locate/msec

The catalytic activity of Ag_2S-montmorillonites as peroxidase mimetic toward colorimetric detection of H_2O_2

Qingyun Liu [a,*], Yanling Jiang [a], Leyou Zhang [a], Xinpei Zhou [a], Xintian Lv [b], Yanyuan Ding [a], Lifang Sun [a], Pengpeng Chen [a], Hailiang Yin [c]

[a] School of Chemistry and Environmental Engineering, Shandong University of Science and Technology, Qingdao 266510, PR China
[b] School of Chemistry and Chemical Engineering, Liaocheng University, Liaocheng 252000, PR China
[c] Academy of Science & Technology, China University of Petroleum, Dongying 257061, PR China

ARTICLE INFO

Article history:
Received 28 October 2015
Received in revised form 22 March 2016
Accepted 1 April 2016
Available online 4 April 2016

Keywords:
Ag_2S
Ca-montmorillonite
Peroxidase
Colorimetric
H_2O_2

ABSTRACT

Nanocomposites based on silver sulfide (Ag_2S) and Ca-montmorillonite (Ca^{2+}-MMT) were synthesized by a simple hydrothermal method. The nanocomposites were characterized by X-ray diffraction (XRD), transmission electron microscopy (TEM) and Fourier transform infrared spectra (FTIR). The as-prepared Ag_2S-MMT nanocomposites were firstly demonstrated to possess intrinsic peroxidase-like activity and could rapidly catalytically oxidize the substrate 3,3′,5,5′-tetramethylbenzidine (TMB) in the presence of H_2O_2 to produce a blue product which can be seen by the naked eye in only one minute. The experimental results revealed that the Ag_2S-MMT nanocomposites exhibit higher thermal durance. Based on the TMB–H_2O_2 catalyzed color reaction, the Ag_2S-MMT nanocomposites were exploited as a new type of biosensor for detection and estimation of H_2O_2 through a simple, cheap and selective colorimetric method.

1. Introduction

Hydrogen peroxide (H_2O_2) is a very important intermediate in environmental and biological reactions. It is widely used in many fields, including pollution control, textile and paper bleaching, sterilization and so on [1–2]. Thus, the rapid and accurate detection of H_2O_2 is of great importance. Good selectivity and high sensitivity can be obtained with H_2O_2 enzymatic biosensors. Peroxidase has great potential for practical application and can be used as a detection kit for H_2O_2 [3]. However, most natural enzymes are proteins and have inherent drawbacks like easy denaturation by environmental changes, digestion by proteases, time-consuming and expensive preparation and purification [4]. In this context, much effort has been devoted for developing artificial enzymes mimetic for practical applications [5]. Among which, nano-scaled materials have attracted increasing interest due to their high specific surface area, small size effect and quantum size effect, which make them have high concentration of low-coordination surface atoms and in turn effective catalytic properties [6–35].

In 2007, Gao et al. [36] reported that Fe_3O_4 nanoparticles (NPs) have an intrinsic enzyme mimetic activity similar to that of natural peroxidases such as horseradish peroxidase (HRP), thus opening the door for the development of nano-scaled inorganic materials in the biochemical field. Some other metal oxide, sulfide and selenide nanomaterials, such as polymer-coated CeO_2 NPs [37], CuO NPs [38,39], Co_3O_4 NPs [40],V_2O_5 nanowires [41], $BiFeO_3$ NPs [42], $CoFe_2O$ NPs [43], sheet-like FeS nanostructure [44], CdS NPs [45], FeS and FeSe NPs [46] were also investigated and found to possess intrinsic peroxidase-like activity. Besides metal oxide nanomaterials, carbon nanomaterials including single-walled [47], helical carbon nanotubes [48], graphene oxide [49] and carbon nanodots [50] displayed intrinsic enzyme mimetic activity. With advantages of low cost, high stability and tunability in catalytic activities, these nanomaterials based peroxidase mimetic have been applied in bioassays and medical diagnostics.

Materials with 2D structures have attracted much attention due to their large surface area and interesting properties [51]. In addition to grapheme [52–54], many inorganic layered compounds with 2D surface such as BN, MoS_2, $TaSe_2$, $MoTe_2$, $MoSe_2$, and $NbSe_2$ give rise to renewed research [55]. Recently, layered double hydroxides (LDHs), such as Co-Fe LDHs, Ni-Al LDH, Co-Al LDH [56–58] were all reported to possess the intrinsic peroxidase-like activity.

The montmorillonite (MMT) has a layered structure and excellent hydrophilic and cation exchange properties. Its layer dimensions in length and width can be in hundreds of nanometers but its thickness is only 1 nm. The MMT layer consists of an octahedral sheet sandwiched between two opposing tetrahedral sheets (TOT), which is called a 2:1 phyllosilicate [59]. These layers are stacked by weak dipolar or Van der Waals forces, and they have both surface and edge charges. Due to

* Corresponding author.
E-mail addresses: qyliu@sdust.edu.cn, qyliusdu@163.com (Q. Liu).

http://dx.doi.org/10.1016/j.msec.2016.04.007
0928-4931/

these structural features, montmorillonite can efficiently behave as a support by introducing many guest species between the layers or on its external surface.

Moreover, silver sulfide (Ag_2S), as a direct semiconductor with a narrow band gap of 1.1 eV, has a relatively large absorption coefficient, leading to its wide application, *i.e.* photoconductors, solar cells, and near infrared photo-detectors [60]. More importantly, Ag_2S is less toxic than other nanoparticles, such as cadmiumsulfide (CdS), lead sulfide (PbS), etc. In fact, compared to the ones based on conventional bulk materials, nanostructured semiconductor materials can lead to a more cost-effective and a less time and energy-consuming solutions [61]. However, to the best of our knowledge, there is no report on the Ag_2S-MMT nanocomposites demonstrating the intrinsic peroxidase-like activity.

In this work, the design and preparation of Ag_2S-MMT nanocomposites were described. The peroxidase-like activity of both pure Ca-montmorillonite and Ag_2S-MMT nanocomposites toward H_2O_2 was investigated. It was found that both pure Ca-montmorillonite (Ca^{2+}-MMT) and Ag_2S-MMT nanocomposites possess intrinsic peroxidase-like activity, and could catalytically oxidize the substrate 3,3′,5,5′-tetramethylbenzidine (TMB) in the presence of H_2O_2 to produce a blue product which can be seen by the naked eye in one minute. Then, the Michaelis–Menten constant of pure Ca^{2+}-MMT and Ag_2S-MMT nanocomposites suggest that the catalytic activity of Ag_2S-MMT nanocomposites is better than that of pure Ca^{2+}-MMT as well as horseradish peroxidase (HRP), indicating that the introduction of Ag_2S tremendously improve Ca^{2+}-MMT's catalytical activity as a peroxidase mimic.

2. Experimental section

2.1. Chemicals

All chemicals used in this work were of analytical grade and used as received without further purification. Silver nitrate ($AgNO_3$) and hydrogen peroxide (30%, H_2O_2) were purchased from Sinopharm Chemical Reagent Co. (Shanghai, China). Thioacetamide (CH_3CSNH_2) and hydrochloric acid (HCl) were purchased from Beijing Chemical Reagent Co. (Beijing, China). 3,3′,5,5′-tetramethylbenzidine (TMB) was purchased from Solarbio (Beijing, China). Acetic acid (HAc) and sodium acetate (NaAc) were purchased from Guangcheng Reagent Co. (Tianjin, China). Ca-montmorillonite was purchased from Tianhong Mining Co. (Mongolia, China).

2.2. Preparation of Ag_2S-MMT nanocomposites

Ag_2S-MMT nanocomposites were prepared according to the previous report [62]. The procedure is as follows: 0.3 g of MMT was dispersed into 30 mL of distilled water under stirring vigorously for 8 h to obtain 1.0% (mass) MMT dispersion. Subsequently, 0.2 mol/L $AgNO_3$ solution with different volume was added stepwise into above suspension under strongly stirring. The molar ratio of Ag^+/montmorillonite was tuned from 0 to 2.0 mmol/g. The mixture was stirred continually for another 3 h at room temperature, assigned solution A. Then, controlled amounts of $AgNO_3$ and thioacetamide (at a molar ratio of 1:6) were dissolved into different volume HCl aqueous solution (0.5 mol/L), assigned B. After that, solution A and B were simultaneously putted into the same sealed container under vigorously stirring for 24 h. The resulting nanocomposites composed of Ag_2S and MMT (Ag_2S-MMT) was then filtered and dried at 65 °C. The pure Ag_2S used as a comparison is obtained under identical experimental conditions.

2.3. Characterization

X-ray powder diffraction (XRD) data were collected using a Rigaku Ultima IV diffractometer (40 kV, Cu Kα (λ = 1.54056 Å); 2θ range 3–70°; scan speed of 5°min^{-1}).The morphology and size distribution of the nanoparticles were studied by using a transmission electron microscope at an accelerating voltage of 200 kV (TEM JEM-2100, JEOL, Japan). Kinetic measurements was carried out on a UV-3200PC UV–vis absorption spectrometer (Shanghai, China). The energy-dispersive X-ray spectrum (EDS) were recorded on an S-4300 (JEOL, Japan) electron microscope, operating at 120 kV. Fluorometric measurements were carried out by a HITACHI F-4600 spectrofluorophotometer (JEOL, Japan).

2.4. Mechanism detection

We presume that the nature of peroxidase-like activities of the Ag_2S-MMT nanocomposites may originate from their catalytic ability to decompose H_2O_2 into ·OH radicals. Therefore, a fluorometric method is used to measure the ·OH radicals using terephthalic acid as a probe. The typical experimental procedure is as follows: H_2O_2 (10 mM), terephthalic acid (0.5 mM) and the Ag_2S-MMT nanocomposites with different concentrations were incubated in acetate buffer (pH 3.8) at 40 °C for 20 min. After centrifugation, the solutions were used for fluorometric measurement.

2.5. Optimization

The peroxidase-like activity of the as-prepared Ag_2S-MMT nanocomposites and pure Ca-montmorillonite was tested by the catalytic oxidation of peroxidase substrate TMB in the presence of H_2O_2. A typical experiment was carried out by using Ag_2S-MMT nanocomposites in a reaction volume of 2.0 mL with 1 mM TMB and 0.25 M H_2O_2 as substrates at room temperature. The blue solutions appeared along with the reaction proceeding were monitored in time scan mode at 652 nm using a spectrophotometer. The influences of the pH value (1.70–10.57), temperature (25–65 °C) and the various concentration

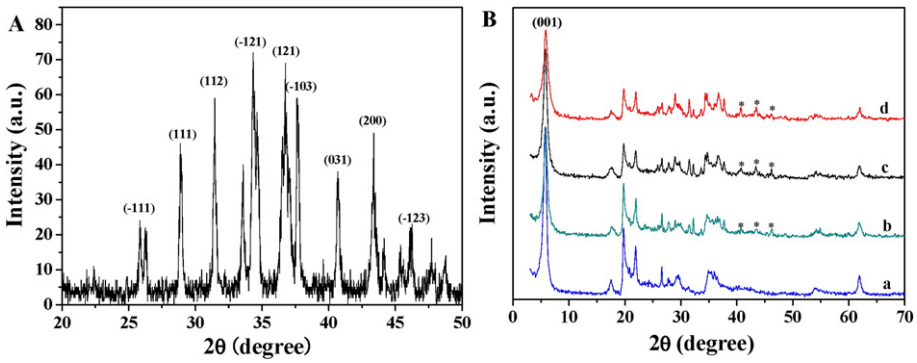

Fig. 1. XRD patterns of: pure Ag_2S (A); (a) pure MMT, (b) 0.5Ag_2S-MMT, (c) 1Ag_2S-MMT, (d) 2Ag_2S-MMT (B).

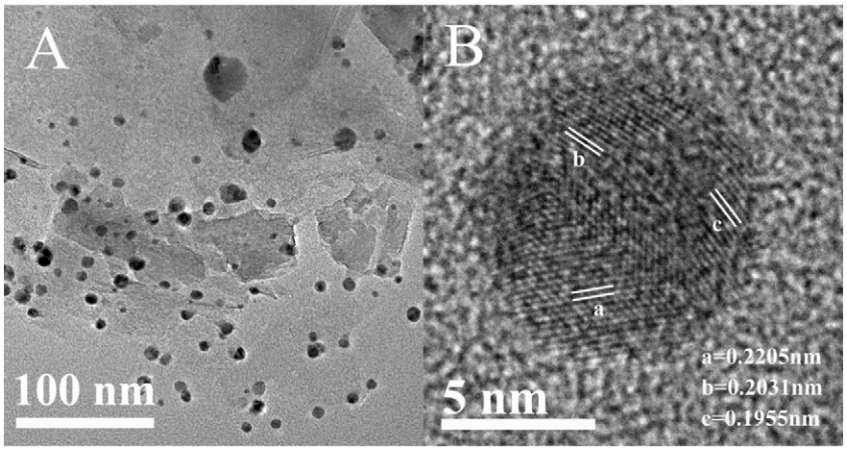

Fig. 2. TEM images of as-prepared Ag_2S-MMT (A), the HRTEM image of Ag_2S NPs (B).

of H_2O_2 were also investigated to evaluate the peroxidase-like activity of Ag_2S-MMT nanocomposites.

2.6. Kinetic analysis

The reaction kinetic measurements were carried out in time course mode by monitoring the absorbance variation at 652 nm [63]. The experiments were carried out with 200 μL of Ag_2S-MMT nanocomposites (0.07 mg·mL^{-1}) or pure MMT in 1.4 mL buffer (HAc-NaAc, pH 3.8) in the presence of 25 mM H_2O_2, using TMB as the substrate. Similarly, when H_2O_2 was used as the substrate, catalytic experiments were performed using 200 μL of Ag_2S-MMT nanocomposites (0.07 mg·mL^{-1}) or pure MMT, 200 μL of TMB (0.1 mM) together with tuning the concentration of H_2O_2 in 1.4 mL HAc-NaAc buffer solution (pH 3.8), keeping a total reaction volume of 2 mL. The concentration of H_2O_2 was tuned to 10, 20, 40, 60, 80, 100, 125 mM for Ag_2S-MMT nanocomposites and 10, 20, 40, 60, 80, 100, 125, 250 mM for pure MMT, respectively. The Michaelis–Menten constant was calculated according to the Michaelis–Menten eqn (1): $v = V_{max}[S]/(K_m + [S])$, where v is the initial velocity, [S] is the concentration of substrate, K_m is the Michaelis constant and V_{max} is the maximal velocity.

2.7. Detection limit (DL)

A typical colorimetric analysis was realized as follows: 200 μL of TMB (0.25 mM), 200 μL of Ag_2S-MMT nanocomposites (0.07 mg·mL^{-1}), and 200 μL of H_2O_2 with various concentrations were added into 1.4 mL of HAc-NaAc buffer (0.026 M, pH 3.8). Then, the mixed solution was used for absorption spectroscopy measurement in time course mode.

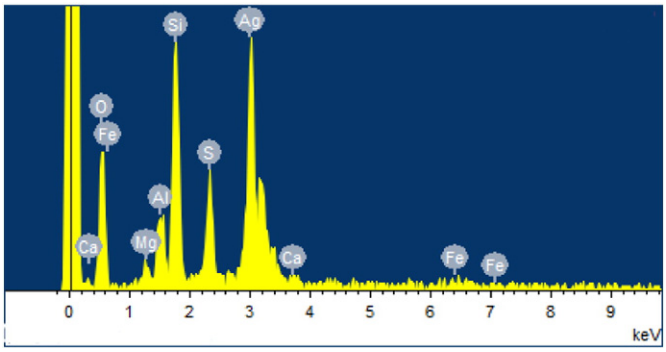

Fig. 3. Energy-dispersive X-ray spectra of Ag_2S-MMT nanocomposites.

3. Results and discussion

3.1. Synthesis and characterization of Ag_2S-MMT nanocomposites

The Ag_2S-MMT nanocomposites were prepared by a simple method. The crystallinity and phase purities of Ag_2S-MMT nanocomposites together with pure Ca-montmorillonite were examined by the powder X-ray diffraction (XRD) technique. The XRD patterns of the Ag_2S-MMT nanocomposites, Ca^{2+}-MMT (Fig. 1A) and pure Ag_2S (Fig. 1B) are shown in Fig. 1. The diffraction peaks of pure Ag_2S show a good match with Ag_2S (JCPDS 14-0072), indicating that the prepared Ag_2S nanomaterials have a monoclinic structure with refined lattice parameters of a = 4.229, b = 6.931, and c = 7.862 Å. These data represent the high crystallinity and fine purity of Ag_2S. As shown in Fig. 1B, the diffraction peaks at 2θ = 40.74°, 43.38° and 46.22° are characteristic for the monoclinic Ag_2S crystal phase. Moreover, the intensity of these peaks becomes stronger with the increasing amount of the added $Ag(NO_3)$. The stronger and sharper diffraction peaks of Ag_2S suggest that the more amount of $Ag(NO_3)$ added, the more Ag_2S crystallites produced.

The morphology and size of the obtained Ag_2S-MMT nanocomposites were characterized by TEM and SEM, shown in Fig. 2 and Fig. S1 (Supporting information). Typical TEM image in Fig. 2A shows that the Ag_2S nanoparticles with the average diameter of ca. 10 nm were dispersed on the surfaces of MMT. Fig. 2B shows the HRTEM image of Ag_2S nanoparticles deposited on montmorillonite (Fig. 2A) which displays clear image of lattice fringes. The interlayer spacings are ca. 0.2205 nm, 0.2031 nm and 0.1955 nm, corresponding to the (031), (200) and (−123) crystal planes of monoclinic Ag_2S, respectively.

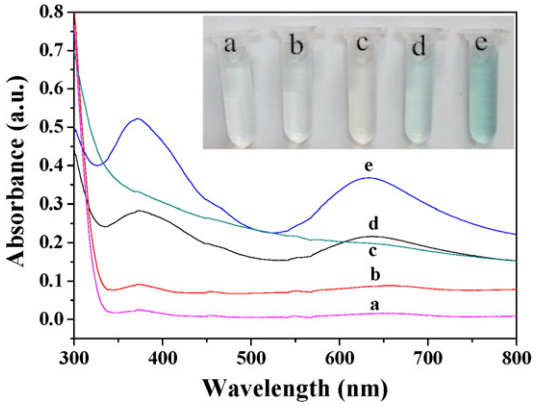

Fig. 4. UV–vis absorption spectra of (a) H_2O_2 + TMB (b) Ag_2S + H_2O_2 + TMB (c) Ag_2S-MMT + TMB (d) MMT + H_2O_2 + TMB (e) Ag_2S-MMT + H_2O_2 + TMB.

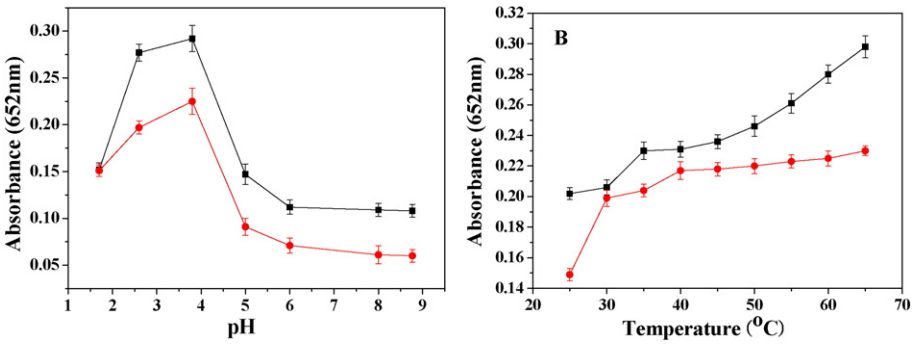

Fig. 5. Dependence of peroxidase-like activity of Ag_2S-MMT nanocomposites (square) and pure MMT (circle) on (A) pH, and (B) temperature.

Fig. 3 displays the energy-dispersive X-ray spectrum (EDS) of Ag_2S-MMT nanocomposites, the dominant peaks of O and Si are due to the MMT. Furthermore, EDS shows the co-existence of Ag and S elements on MMT with the atomic ratio of Ag to S of 10.68:5.31, which is close to the stoichiometric ratio (2:1) of the precursors, strongly suggesting the presence of Ag_2S species in the sample.

3.2. Peroxidase-like activity of Ag_2S-MMT nanocomposites

To investigate the peroxidase-like activity of Ag_2S-MMT nanocomposites and pure MMT, the catalytic oxidation of peroxidase substrate TMB was tested in the presence of H_2O_2. The maximum absorbance of oxTMB is at 652 nm [63]. Fig. 4 shows photographs of different reaction systems. It can be observed that additional control experiments using TMB in the absence of Ag_2S-MMT composite or H_2O_2 show no obvious color change, indicating that the two components are required for the reaction (Fig. 4). It can also be seen that the catalytic activity of Ag_2S-MMT was much higher than that of pure MMT, revealing that an activated sample of Ag_2S-MMT exhibited enhanced peroxidase-like catalytic activity under identical conditions.

3.3. Optimization of the reaction conditions

Similar to natural peroxidases such as HRP, the catalytic activity of Ag_2S-MMT nanocomposites and pure MMT is dependent on pH, temperature and other experimental conditions [36]. Influences of pH and temperature on the catalytic activity of Ag_2S-MMT nanocomposites and pure MMT were studied through varying the pH (from 1.70 to 8.77) and the temperature (from 25 °C to 70 °C), respectively.

Fig. 5 shows the pH- and temperature-dependent response curves, respectively. Clearly, the activity of the Ag_2S-MMT nanocomposites was higher than that of pure MMT in the wide range of pH and temperature, respectively. The optimal pH was approximately 3.8 for Ag_2S-MMT nanocomposites and pure MMT, which are similar to that of Fe_3O_4 magnetic nanoparticles [64] and $C_{60}[C(COOH)_2]_2$ [65]. Thus, pH 3.8 was adopted as standard conditions for the subsequent analysis of Ag_2S-MMT nanocomposites and pure MMT on catalytic activity. Furthermore, it can be found that the catalytic activity of Ag_2S-MMT nanocomposites was much higher in weakly acidic solutions than that in neutral, indicating that the oxidation reaction of TMB occurred easily under weakly acidic conditions, which is similar to those of other nanomaterials [28,29,64] and HRP [63]. From Fig. 5B, it can be seen that the catalytic activity of the Ag_2S-MMT nanocomposites and pure MMT was always rising with the increase of experimental temperature while it was not inhibited at a high temperature, indicating that the catalytic activity of the Ag_2S-MMT nanocomposites and pure MMT was more stable at high temperature than that of HRP (Fig. S2, Supporting information).

Table 1
Comparison of the apparent Michaelis constant (K_m) and maximum reaction rate (V_m).

Catalyst	K_m [mM]		$V_m[10^{-8}Ms^{-1}]$	
	H_2O_2	TMB	H_2O_2	TMB
MMT	3.053 ± 1.055	0.01097 ± 0.002	1.818 ± 0.224	1.797 ± 0.022
Ag_2S-MMT	1.874 ± 0.035	0.00412 ± 0.0003	2.286 ± 0.048	5.27 ± 0.008
HRP [36]	3.7	0.434	5.31	13.08

3.4. Steady-state kinetics assay

The catalytic activity of the Ag_2S-MMT nanocomposites and pure MMT was further investigated by enzyme kinetics theory methods with H_2O_2 and TMB as substrates under the optimum conditions [66]. The kinetic data were obtained by varying one substrate concentration and fixing the other as a constant. A series of initial reaction rates were calculated based on the double reciprocal of the Michaelis–Menten equation, $1/v_0 = K_m/V_{max}(1/[S] + 1/K_m)$ [67]. The K_m and V_{max}, obtained from Lineweaver–Burk plots were listed in Table 1. As can be seen from Fig. 6, within a particular range of substrate concentration, the reaction was consistent with typical Michaelis–Menten kinetics. The K_m value of the pure MMT with H_2O_2 as the substrate is higher than that of Ag_2S-MMT nanocomposites, which is in accordance with the result of the maximal activity of the pure MMT obtained in a higher H_2O_2 concentration. Nevertheless, the K_m values of pure MMT with TMB as the substrate is higher than that of the Ag_2S-MMT nanocomposites, suggesting that pure MMT has a lower affinity for TMB. Further, in comparison with that of HRP [36] (Table 1), the pure MMT and Ag_2S-MMT nanocomposites show a lower K_m value with H_2O_2 or TMB as the substrate, indicating that pure MMT and Ag_2S-MMT nanocomposites have a better affinity for any substrate than HRP [36].

3.5. Mechanism of peroxidase-like activity of Ag_2S-MMT nanocomposites

The peroxidase-like catalytically activated mechanism of Ag_2S-MMT nanocomposites was investigated by using terephthalic acid as a fluorescence probe to evaluate the effects of Ag_2S-MMT nanocomposites on $^{\bullet}OH$ signal intensity. Hydroxyl radicals cannot be detected directly because of its short lifetime. However, it reacts readily with terephthalic acid, forming highly fluorescent 2-hydroxyterephthalic acid that can be identified from fluorescence spectrometer [68]. The fluorescence intensity increased with the addition of Ag_2S-MMT nanocomposites (Fig. 7), suggesting that the amount of generated $^{\bullet}OH$ radicals increased with the amount of Ag_2S-MMT nanocomposites. This indicates that Ag_2S-MMT nanocomposites could catalyze H_2O_2 decomposition into $^{\bullet}OH$ radicals. Therefore, the nature of peroxidase-like activity of the Ag_2S-MMT nanocomposites should originate from $^{\bullet}OH$ radicals generation. However, the fluorescence intensity of the system decreased with an increasing concentration of nanocomposites was due to the competitive relation between Ag_2S-MMT nanocomposites and terephthalic acid in capturing

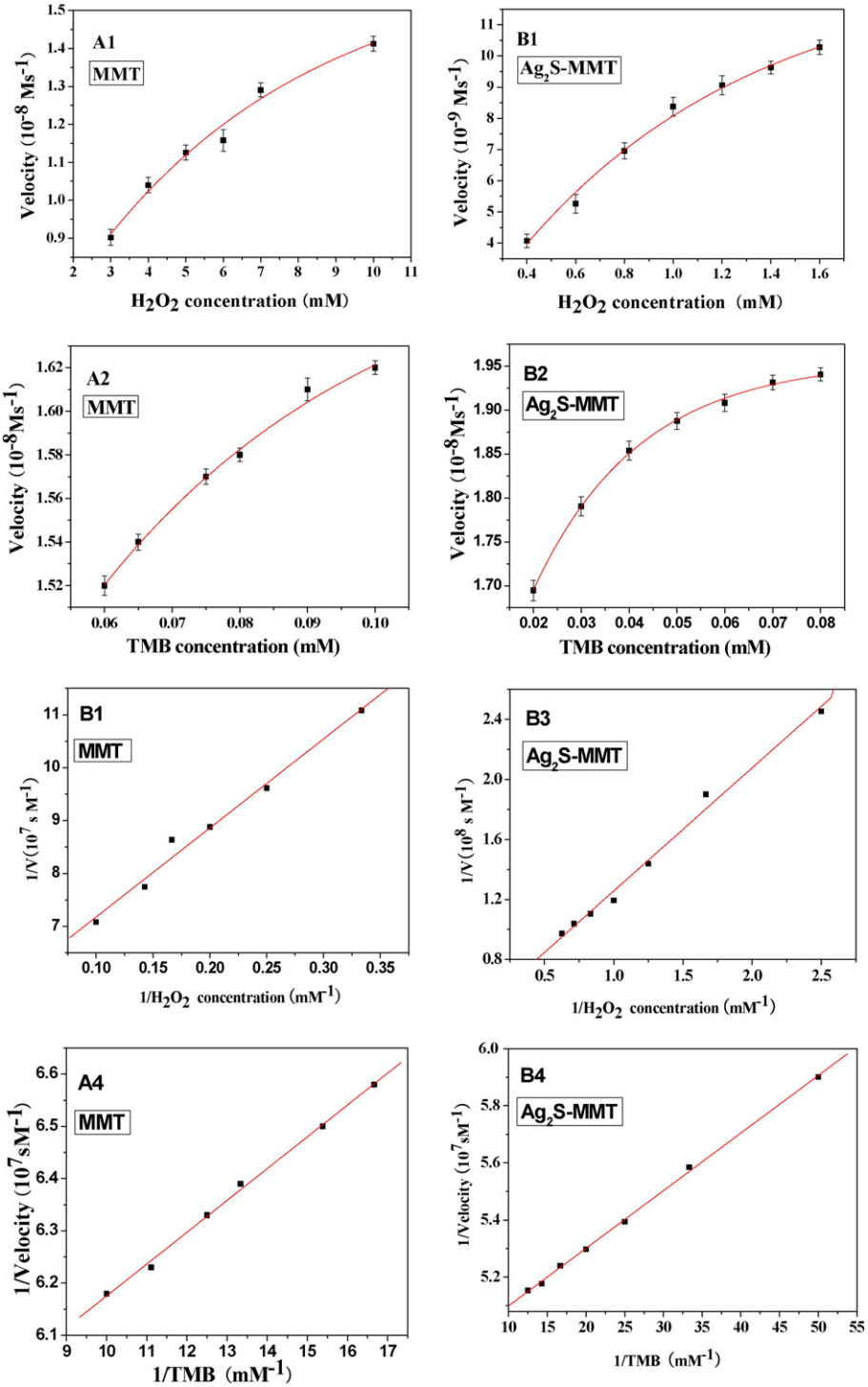

Fig. 6. Lineweaver–Burk plots of pure MMT H_2O_2 as substrate (A3) TMB as substrate (A4) and Ag_2S-MMT nanocomposites H_2O_2 as substrate (B3) TMB as substrate (B4). Steady-state kinetic assay (A1, B1, A2, B2). The concentration of TMB·2HCl was 0.1 mM and the H_2O_2 concentration was varied (a1 and b1). The concentration of H_2O_2 was 10 mM and the TMB·2HCl concentration was varied (a2 and b2).

•OH radicals. The competitive ability of terephthalic acid in •OH radicals decreased with an increasing concentration of Ag_2S-MMT nanocomposites, resulting in the fluorescence intensity decreased.

3.6. Detection of H_2O_2

A colorimetric method for detection of H_2O_2 was developed on the basis of the intrinsic catalytic activity of Ag_2S-MMT nanocomposites. Because the absorbance at 652 nm of oxidized TMB is in proportion to the H_2O_2 concentration, H_2O_2 can be simply detected by the naked eye or using a UV–vis spectrometer. Fig. 8A shows the time-course dependent absorbance changes at 652 nm of oxidized TMB in the presence of different concentrations of H_2O_2. Fig. 7B represents the H_2O_2 concentration–response curves under experimental conditions. The linear range is from 0.2 mM to 1.2 mM with a detection limit (DL) of 1.916×10^{-5} mol·L^{-1}. The linear regression equation is A = 0.24313 + 0.10413C (mM) and the correlation coefficient r is 0.9983. The detection limit is lower than that of previously reported Au@Pt

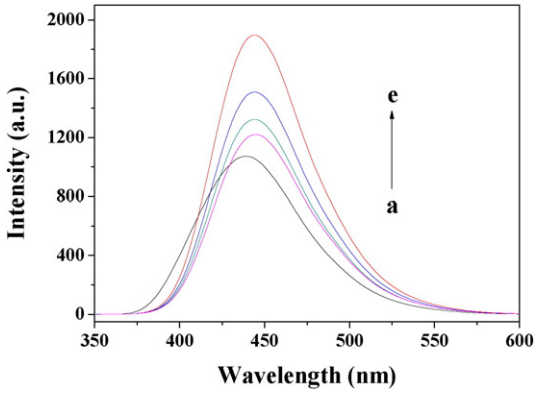

Fig. 7. The effect of the Ag_2S-MMT composites on the formation of hydroxyl radical with terephthalic acid as a fluorescence probe. a–e: 0, 80, 70, 60, 20 $\mu g \cdot mL^{-1}$ Ag_2S-MMT composites.

core-shell na-norods (4.5×10^{-5} M) [69], indicating that Ag_2S-MMT nanocomposites have better response toward H_2O_2 detection. Meanwhile, the low LOD can agree well with the result that the Ag_2S-MMT nanocomposites have a higher affinity for H_2O_2 in our system. Therefore, the sensor based on Ag_2S-MMT nanocomposites could be suitable for detection of H_2O_2.

3.7. Application in real sample analysis

To validate the practical application of our proposed colorimetric method in real sample, the determination of hydrogen peroxide in the milk samples purchased from the supermarket in Qingdao (China) was executed under optimal conditions. The milk samples were spiked with different concentration of hydrogen peroxide (Table 2) and the analysis of same real sample was repeatedly measured for 6 times. As listed in Table 2, the comparisons were made between spiked and obtained values, which no significant differences were observed. According to the calibration curve for hydrogen peroxide (Fig. 8B). The recovery rates are 95.3, 102, 98.6%, respectively. This shows the feasibility and potential of the method for real sample analysis.

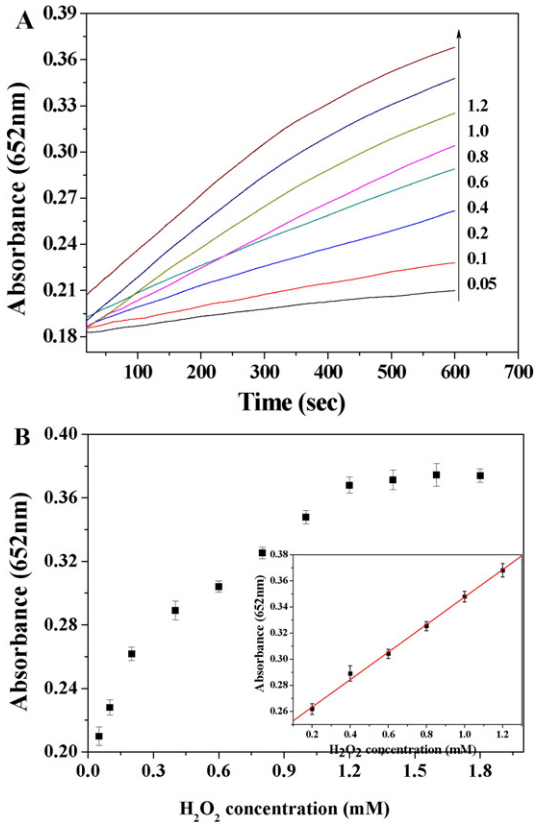

Fig. 8. (A) Time-dependent absorbance changes at 652 nm of TMB reaction solutions catalyzed by Ag_2S-MMT nanocomposites in the presence of different concentrations of H_2O_2 at room temperature. (B) A dose–response curve for H_2O_2 detection. Inset: linear calibration plot for H_2O_2.

Table 2
Determination of H_2O_2 in milk samples in the presence of Ag_2S-MMT.

Milk samples	Detected (μM)	Added (μM)	Found (μM)	Recovery (%)	RSD (%)
1	No detection	300.0	285.9	95.3	1.87
2	No detection	500.0	510	102	1.01
3	No detection	600.0	591.4	98.6	0.68

4. Conclusions

In summary, Ag_2S-MMT nanocomposites as peroxidase mimetics were prepared by a simple and green method. The nanocomposites could catalytically oxide peroxidase substrate TMB in the presence of H_2O_2 in a short time (only 1 min) and could be observed by the naked eye. The Ag_2S-MMT nanocomposites have demonstrated the brilliant enhanced peroxidase-like activity compared to pure MMT. The activity of the Ag_2S-MMT nanocomposites are dependent on pH, temperature, amount of Ag_2S-MMT nanocomposites and H_2O_2 concentration, respectively. As a result, a colorimetric detection for H_2O_2 using the nanocomposites as catalysts was proposed which can be used for H_2O_2 determination.

Acknowledgements

This work was financially supported by the National Natural Science Foundation of China (Grant No. 21271119 and 21206197) and Promotive Research Fund for Excellent Young and Middle-aged Scientists of Shandong Province (BS2013CL021).

Appendix A. Supplementary data

Supplementary data to this article can be found online at http://dx.doi.org/10.1016/j.msec.2016.04.007.

References

[1] H. Notsu, T. Tatsuma, A. Fujishima, J. Electroanal. Chem. 523 (2002) 86–92.
[2] C.G. Tsiafoulis, P.N. Trikalitis, M.I. Prodromidis, Electrochem. Commun. 7 (2005) 1398–1404.
[3] Y.J. Song, K.G. Qu, C. Zhao, J.S. Ren, X.G. Qu, Adv. Mater. 22 (2010) 2206–2210.
[4] E. Shoji, M.S. Freund, J. Am, Chem. Soc. 123 (2001) 3383–3384.
[5] R. Breslow, Acc. Chem. Res. 28 (1995) 146–153.
[6] X.Q. Zhang, S.W. Gong, Y. Zhang, T. Yang, C.Y. Wang, J. Mater. Chem. 20 (2010) 5110–5116.
[7] W.B. Shi, X.D. Zhang, S.H. He, Y.M. Huang, Chem. Commun. 47 (2011) 10785–10787.
[8] X. Zuo, C. Peng, Q. Huang, S. Song, L. Wang, D. Li, Nano Res. 2 (2009) 617–623.
[9] J.B. Liu, X.N. Hu, S. Hou, T. Wen, W.Q. Liu, X. Zhu, X.C. Wu, Chem. Commun. 47 (2011) 10981–10983.
[10] S.H. Liu, F. Lu, R.M. Xing, J.J. Zhu, Chem. Eur. J. 17 (2011) 620–625.
[11] H.Y. Niu, D. Zhang, S.X. Zhang, X.L. Zhang, Z.F. Meng, Y.Q. Cai, J. Hazard. Mater. 190 (2011) 559–565.
[12] S.H. He, W.B. Shi, X.D. Zhang, J. Li, Y.M. Huang, Talanta 82 (2010) 377–383.
[13] W.W. He, X.C. Wu, J.B. Liu, X.N. Hu, K. Zhang, S. Hou, W.Y. Zhou, S.S. Xie, Chem. Mater. 22 (2010) 2988–2994.
[14] K. Park, M. Kim, H. Park, Small 7 (2011) 1521–1525.
[15] N. Wang, L. Zhu, M. Wang, D. Wang, H. Tang, Ultrason. Sonochem. (2009) 4–9.
[16] C. Korsvik, S. Patil, S. Seal, W. Self, Chem. Commun. (2007) 1056–1058.

[17] E. Heckert, A. Karakoti, S. Seal, W. Self, Biomaterials 29 (2008) 2705–2709.
[18] A. Asati, S. Santra, C. Kaittanis, S. Nath, J. Perez, Angew. Chem. Int. Ed. 48 (2009) 2308–2312.
[19] T. Pirmohamed, J. Dowding, S. Singh, B. Wasserman, E. Heckert, A. Karakoti, Chem. Commun. 46 (2010) 2736–2738.
[20] R. Andre, F. Natalio, M. Humanes, J. Leppin, K. Heinze, R. Wever, H. Schroder, Adv. Funct. Mater. 21 (2011) 501–509.
[21] Y. Jv, B. Li, R. Cao, Chem. Commun. 46 (2010) 8017–8019.
[22] J. Fan, J. Yin, B. Ning, X. Wu, Y. Hu, M. Ferrari, G. Anderson, J. Wei, Y. Zhao, G. Nie, Biomaterials 32 (2011) 1611–1618.
[23] W. He, Y. Liu, J. Yuan, J. Yin, X. Wu, X. Hu, K. Zhang, J. Liu, Biomaterials 32 (2011) 1139–1147.
[25] Q. Wang, Y. Chen, P. Ma, J. Lu, X. Zhang, J. Jiang, J. Mater. Chem. 21 (2011) 8057–8806.
[26] X. Wang, K. Qu, B. Xu, J. Ren, X. Qu, Nano Res. 4 (2011) 908–920.
[27] X. Wang, Q. Wu, Z. Shan, Q. Huang, Biosens. Bioelectron. 26 (2011) 3614–3619.
[28] S. Song, Y. Qin, Y. He, Q. Huang, C. Fan, H.Y. Chen, Chem. Soc. Rev. 39 (2010) 4234–4243.
[29] Y. Song, K. Qu, C. Zhao, J. Ren, X. Qu, Adv. Mater. 22 (2010) 2206–2210.
[30] R. Cui, Z. Han, J. Zhu, Chem. Eur. J. 17 (2011) 9377–9384.
[31] F. Qu, T. Li, M. Yang, Biosens. Bioelectron. 26 (2011) 3927–3931.
[32] Y. Song, Y. Chen, L. Feng, X. Qu, Chem. Commun. 47 (2011) 4436–4438.
[33] Y. Song, W. Wei, X. Qu, Adv. Mater. 23 (2011) 4215–4236.
[34] Y. Lee, M. Garcia, N. Huls, H. Sun, Angew. Chem. Int. Ed. 49 (2010) 1271–1274.
[35] H. Wei, E. Wang, Chem. Soc. Rev. 42 (2013) 6060–6093.
[36] L. Gao, J. Zhuang, L. Nie, J.B. Zhang, Y. Zhang, N. Gu, T.H. Wang, J. Feng, D.L. Yang, S. Perrett, X.Y. Yan, Nat. Nanotechnol. 2 (2007) 577–583.
[37] A. Asati, S. Santra, C. Kaittanis, S. Nath, J.M. Perez, Angew. Chem. Int. Ed. 48 (2009) 2308–2312.
[38] W. Chen, J. Chen, A.L. Liu, L.M. Wang, G.W. Li, X.H. Lin, Chem. Cat. Chem. 3 (2011) 1151–1154.
[39] W. Chen, J. Chen, Y.B. Feng, L. Hong, Q.Y. Chen, L.F. Wu, X.H. Lina, X.H. Xia, Analyst 137 (2012) 1706–1712.
[40] J. Mu, Y. Wang, M. Zhao, L. Zhang, Chem. Commun. 48 (2012) 2540–2542.
[41] R. Andre, F. Natalio, M. Humanes, J. Leppin, K. Heinze, R. Wever, H.C. Schroeder, W.E.G. Mueller, W. Tremel, Adv. Funct. Mater. 21 (2011) 501–509.
[42] W. Luo, Y.S. Li, J. Yuan, L. Zhu, Z. Liu, H. Tang, S. Liu, Talanta 81 (2010) 901–907.
[43] W. Shi, X. Zhang, S. He, Y. Huang, Chem. Commun. 47 (2011) 10785–10787.
[44] Z. Dai, S. Liu, J.H. Ju, Chem. Eur. J. 15 (2009) 4321–4326.
[45] S.K. Maji, A.K. Dutta, D.N. Srivastava, P. Paul, A. Mondal, B. Adhikary, J. Mol. Catal. A Chem. 358 (2012) 1–9.
[46] A.K. Dutta, S.K. Maji, D.N. Srivastava, A. Mondal, P. Biswas, P. Paul, B. Adhikary, ACS Appl. Mater. Interfaces 4 (2012) 1919–1927.
[47] Y.J. Song, X.H. Wang, C. Zhao, K.G. Qu, J.S. Ren, X.G. Qu, Chem. Eur. J. 16 (2010) 3617–3621.
[48] R.J. Cui, Z.D. Han, J.J. Zhu, Chem. Eur. J. 17 (2011) 9377–9384.
[49] Y.J. Song, K.G. Qu, C. Zhao, J.S. Ren, X.G. Qu, Adv. Mater. 22 (2010) 2206–2210.
[50] W.B. Shi, Q.L. Wang, Y.J. Long, Z.L. Cheng, S.H. Chen, H.Z. Zheng, Y.M. Huang, Chem. Commun. 47 (2011) 6695–6697.
[51] M. Osada, T. Sasaki, J. Mater. Chem. 19 (2009) 2503–2511.
[52] J. Li, J. Yang, Z. Yang, Y. Li, S. Yu, Q. Xu, X. Hu, Anal. Methods 4 (2012) 1725–1728.
[53] T. Kuila, S. Bose, P. Khanra, A.K. Mishra, N.H. Kim, J.H. Lee, Biosens. Bioelectron. 26 (2011) 4637–4648.
[54] Y. Song, K. Qu, C. Zhao, J. Ren, X. Qu, Adv. Mater. 22 (2010) 2206–2210.
[55] R.J. Smith, P.J. King, M. Lotya, C. Wirtz, U. Khan, S. De, A. O'Neill, G.S. Duesberg, J.C. Grunlan, G. Moriarty, J. Chen, J. Wang, A.I. Minett, V. Nicolosi, J.N. Coleman, Adv. Mater. 23 (2011) 3944–3948.
[56] Y.W. Zhang, J.Q. Tian, S. Liu, Analyst 137 (2012) 1325–1328.
[57] H.H. Ai, X.T. Huang, Z.H. Zhu, Biosens. Bioelectron. 24 (2008) 1048–1052.
[58] L.J. Chen, B. Sun, X.D. Wang, J. Mater. Chem. B 1 (2013) 2268–2274.
[59] M.F. Brigatti, E. Galan, B.K.G. Theng, Structure and mineralogy of clay minerals, in: F. Bergaya, G.K.B. Theng, G. Lagaly (Eds.), Handbook of Clay Science, Developments in Clay Science, 1, Elsevier, Amsterdam 2006, pp. 19–86.
[60] K. Skalska, J.S. Miller, S. Ledakowicz, A review, Sci. Total Environ. 408 (2010) 3976–3989.
[61] J.E. Hutchison, ACS Nano 2 (2008) 395–402.
[62] H. Boukhatem, L. Djouadi, N. Abdelaziz, H. Khalaf, Appl. Clay Sci. 72 (2013) 44–48.
[63] P. Josephy, T. Eling, R. Mason, J. Biol. Chem. 257 (1982) 3669–3675.
[64] H. Wei, E. Wang, Anal. Chem. 80 (2008) 2250–2254.
[65] X. Li, Y. Zhong, Q. Li, L. Wang, J. Colloid Interface Sci. 405 (2013) 226–232.
[66] M. Frasconi, G. Favero, C. Tortolini, Electroanalysis 21 (2009) 2378–2386.
[67] P. Atkins, J. Paula, Elements of Physical Chemistry, Oxford University Press, Oxford, UK, 2006.
[68] K. Ishibashi, A. Fujishima, T. Watanabe, K. Hashimoto, Photochem. Photobiol. A 134 (2000) 139–142.
[69] J. Liu, X. Hu, S. Hou, T. Wen, W. Liu, X. Zhu, J.J. Yin, X. Wu, Sensors Actuators B Chem. 166–167 (2012) 708–714.